International Research Journal of Engineering and Technology (IRJET) e-ISSN: 2395-0056
Volume: 10 Issue: 05 | May 2023 www.irjet.net p-ISSN: 2395-0072

STRESS ANALYSIS & OPTIMIZATION OF A LOWER CONTROL ARM OF SUSPENSION SYSTEM BY USING OPTISTRUCT

Ranshing Aishwarya Sanjeev[1], Amol B Gaikwad[2], Kharad B.N.[3]

[1]Sholar,Dept of Mechanical Engg, Vishwabharti Academy's College of Engineering, Ahmednagar, Maharashtra, India
[2]Asst. Prof. Dept of Mechanical Engg, Dr. D.Y.Patil School of Engineering, Pune, Maharashtra, India
[3]Asst. Prof. Dept of Mechanical Engg, Vishwabharti Academy's College of Engineering, Ahmednagar, Maharashtra, India

---

Abstract:

The lower control arm is a critical component in the suspension system of an automobile, responsible for supporting the weight of the vehicle and maintaining stability during various driving conditions. This abstract presents a systematic approach towards the optimization of the lower control arm design, aiming to enhance its performance and reliability while considering factors such as weight reduction, material selection, and structural integrity. The optimization process begins with a comprehensive review of existing lower control arm designs, identifying their strengths and limitations. Next, various design parameters are identified and evaluated, including geometric dimensions, material properties, and attachment points. Utilizing advanced computer-aided design (CAD) software and simulation tools, a virtual model of the lower control arm is created to assess its structural behavior under different loading scenarios.

1. INTRODUCTION

1.1 Suspension System

Suspension refers to the collection of springs, shock absorbers, and linkages that establish a connection between a vehicle and its wheels, enabling relative motion between the two. It serves a dual function by enhancing the vehicle's road holding, handling, and braking performance for improved active safety and driving enjoyment, while also providing a comfortable and isolated environment for occupants, reducing road noise, bumps, and vibrations. Achieving these objectives often requires striking a balance, as they can conflict with each other. Therefore, optimizing suspension systems involves finding the appropriate compromise that meets the desired outcomes.

1.2 Lower Control Arm

The lower control arm is an essential component of the MacPherson suspension system commonly found in vehicles. In most front suspensions, two control arms, often referred to as lower control arms, are present. However, certain vehicles like the Honda Accord and many trucks have four control arms, consisting of two upper and two lower arms. These control arms serve the purpose of connecting the car's frame or body to the assembly that holds the front wheel, known as the steering knuckle. To enable flexibility, the control arms are attached to the frame or body of the car using rubber bushings called control arm bushings.

Figure: 1.1 Lower control Arm

1.3 Problem Statement

The unsprung weight of a wheel plays a crucial role in striking a balance between its ability to follow bumps and isolate vibrations. If a wheel is heavier and moves less, it will not absorb vibrations effectively, resulting in the transfer of road surface irregularities to the cabin through the suspension geometry. As a result, ride quality and road noise are adversely affected. Additionally, when the wheels encounter longer bumps, a higher unsprung mass leads to increased energy absorption by the wheels, further deteriorating the ride experience.

Furthermore, excessive unsprung weight poses challenges in wheel control during intense acceleration or braking. It

can cause wheel hop, negatively impacting traction and steering control.

1.4 Objective

- Perform static structural analysis of the existing lower control arm model using ANSYS Workbench, a finite element analysis (FEA) software.
- Conduct topological optimization of the lower control arm using the OPTISTRUCT solver. This optimization process aims to improve the design by considering factors such as weight reduction and material cost.
- Optimize the lower control arm design to achieve a weight reduction of up to 15 to 20% while maintaining the required factor of safety. Additionally, propose alternative designs that meet the permissible limits of safety.
- Compare the factor of safety between the optimized design and the baseline design of the lower control arm.
- Validate the results obtained from the FEA analysis by conducting experimental tests and ensuring their consistency and accuracy.

1.5 Conclusion from Literature Review:

Based on previous studies, it is evident that while there have been numerous works conducted on Wishbone and MacPherson suspension systems, the majority of them have focused on improving efficiency and performance. It is also worth noting that the literature primarily consists of analytical studies employing finite element analysis to examine various suspension components. However, there has been limited research exploring the weight optimization specifically of the lower control arm.

2. THEORETICAL ANALYSIS

2.1 Dimension of Lower Control arm

The design data sheet of the lower control arm is provided in the appendix. The dimensions of the existing lower control arm, sourced from a WagonR car, are presented in Figure 2.1. The lower control arm has an overall length of 463mm, a width of 241.9mm, and a thickness of 3mm.

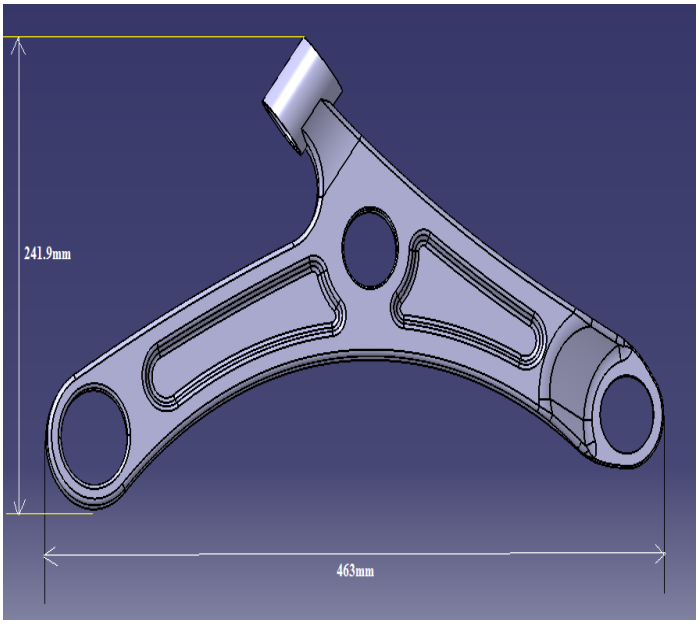

Figure: 2.1 Dimension of Lower Control Arm

2.2 Material properties

Lower control arms are subjected to significant load carrying requirements, necessitating a material with high strength and durability. The existing component utilizes AISI 1040 material, which is a type of steel. Steel is a suitable material choice due to its desirable properties such as a high yield point, elasticity, and buckling strength, among others [6]. These characteristics make steel an ideal material for meeting the demanding mechanical requirements of lower control arms.

Table 2.1 Material Properties of AISI 1040

Sr. No.	Description	Values
1	Modulus of Elasticity	2.1e5 MPa
2	Poisson's Ratio	0.3
3	Yield Strength	415 MPa
4	Density	7850 Kg/m^3
5	Tensile strength	620 MPa

3. FINITE ELEMENT ANALYSIS

The finite element method (FEM) is a numerical technique employed to approximate solutions for boundary value problems associated with partial differential equations. It is commonly known as finite element analysis (FEA) and involves dividing a complex problem into smaller, more manageable parts known as finite elements.

In the case of the control arm, it is necessary to mesh the conventional model developed in modeling software for analysis purposes. The control arm is meshed using tetrahedral elements, ensuring that the model is properly divided for analysis. The mesh model, as depicted in Figure 3.1, employs solid tetrahedral elements for the control arm.

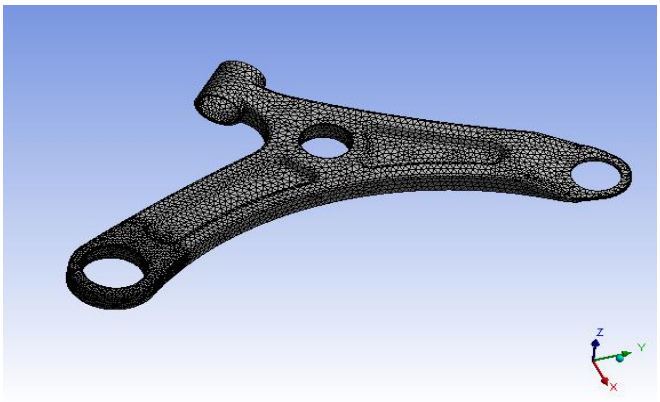

Figure: 3.1 Meshing of Lower Control Arm

3.1 Analysis Result of Baseline model

The baseline control arm exhibits a maximum displacement of 6.02 mm. According to the distortion energy theory, the maximum equivalent stress observed in the lower arm model is 344 MPa. The yield strength of the material used is 415 MPa. The results indicate that the von-Mises stress of 344 MPa is lower than the yield strength of the material. Consequently, the factor of safety for the baseline lower arm is calculated as 1.2.

3.2 Deformation Analysis:

The contour plots displaying the displacement distribution are presented in Figure 3.2. It is observed that the maximum displacement exhibited by the baseline lower control arm is 6.02mm. This displacement is primarily concentrated at the ball joint end, while no significant deformation is detected at the fixed and turning ends of the control arm.

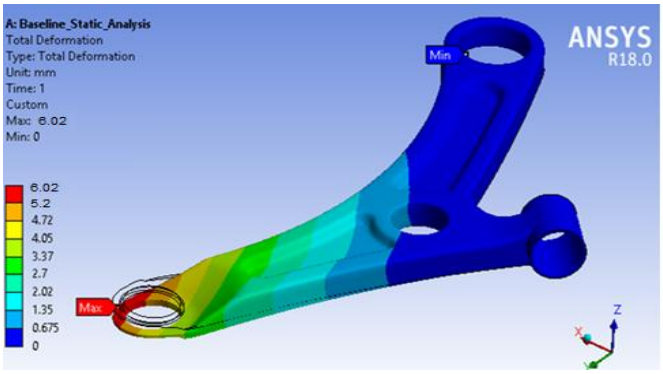

Figure: 3.2 Maximum deformation Plot of Baseline model

3.3tress Analysis: The following figure 3.3 shows contour plot of the von-Mises stress. As per distortion energy theory, the maximum equivalent stress observed in the lower arm model is 344 MPa.

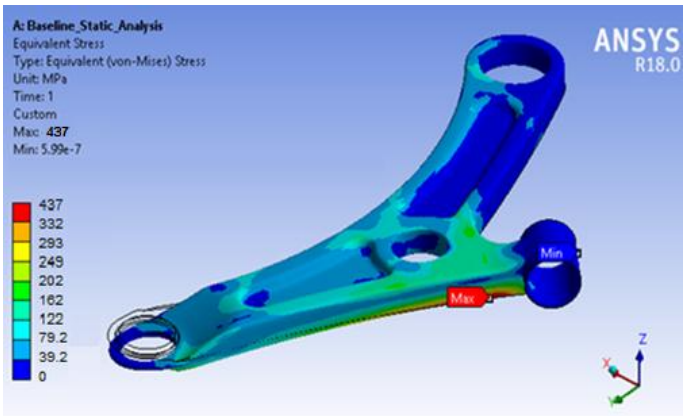

Figure: 3.3 Equivalent Stress Plot of Baseline model

From the above analysis it is found that Von-Mises stress is maximum nearer to turning joint. Also it is found that minimum stress is generated at ball joint and fixed end.

3.4Factor of Safety:

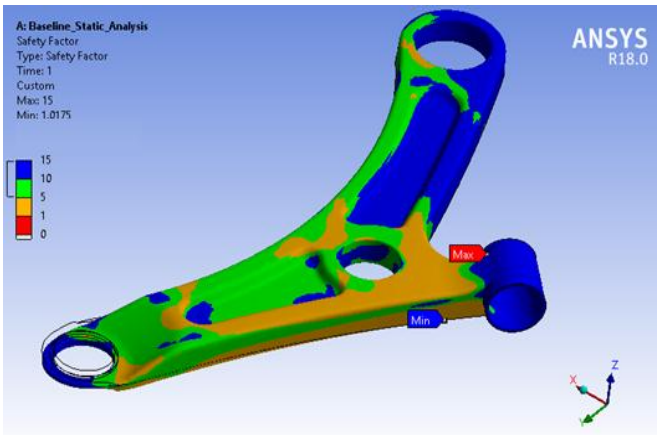

Figure: 3.4 Plot of Factor of Safety of Baseline model

The material used in the lower control arm has a yield strength of 415 MPa. The analysis results indicate that the von-Mises stress in the baseline model is 344 MPa, which is below the yield strength of the material. As a result, the factor of safety for the baseline lower arm is calculated as 1.2. These findings suggest that there is room for optimization and potential for reducing the weight or improving the performance of the lower control arm while maintaining safety factors within acceptable limits.

Following table 3.1 shows FEA result analysis of baseline model.

Table 3.1 FEA Result Analysis of Baseline model

Method	Description	Baseline Design
FEA Method	Deflection (mm)	6.02
	Von-Mises stress (MPa)	344
	Factor of Safety	1.2
	Mass (Kg)	1.2

3.5 Optimization of Lower Control Arm

Optimization is a process that involves identifying the most cost-effective or highest-performing alternative within given constraints. It aims to maximize desired factors while minimizing undesired ones. In contrast, maximization refers to the act of achieving the highest or maximum result or outcome without considering the associated costs or expenses.

4 OPTISTRUCT MODEL

The optimized CAD is prepared in the modeling software. The same CAD is exported in ".step" format and imported in HYPERMESH.

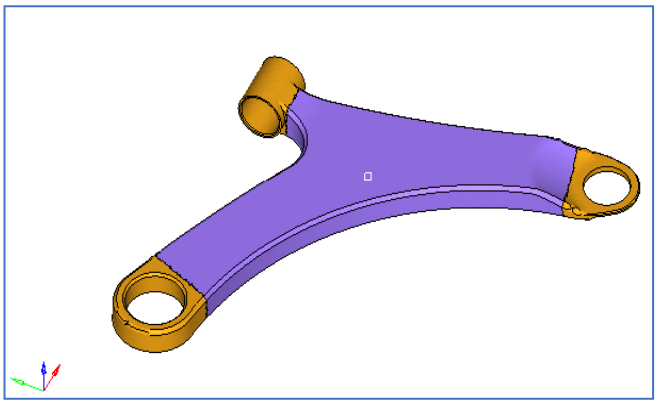

Figure: 4.1 CAD Used for Optimization

The optimized CAD model is meshed in HYPERMESH with CTETRA elements. Following figure 4.2 shows the mesh model for optimization.

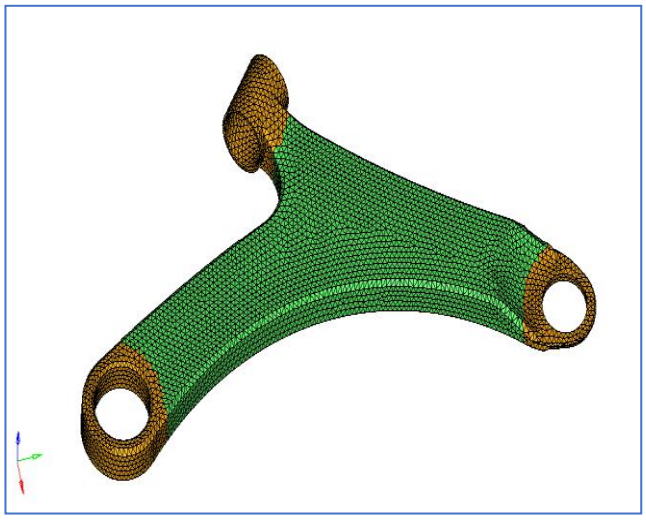

Figure: 4.2 Mesh Model for Optimization

For carrying out an optimization, first whole body surface is filled with material and then same boundary condition is applied which is as shown in figure 4.3

4.1 Boundary Conditions

The boundary conditions include restraining rigid body motion, applying force on another end of the control arm up to 750N,

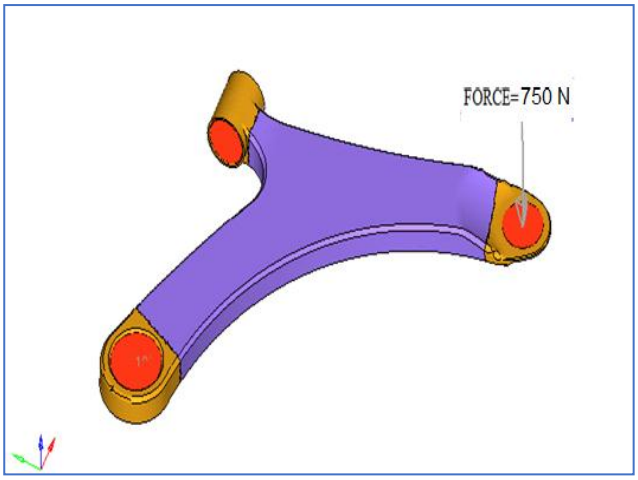

Figure: 4.3 Boundary Conditions for Topology optimization

4.2 Analysis Result for Optimized Model

The element density plot provides an optimized pattern for the model, indicating areas within the lower control arm where material can be removed from the design. This optimized design is derived from the initial design obtained through analysis. The preparation of the optimized design is carried out using CATIA software.

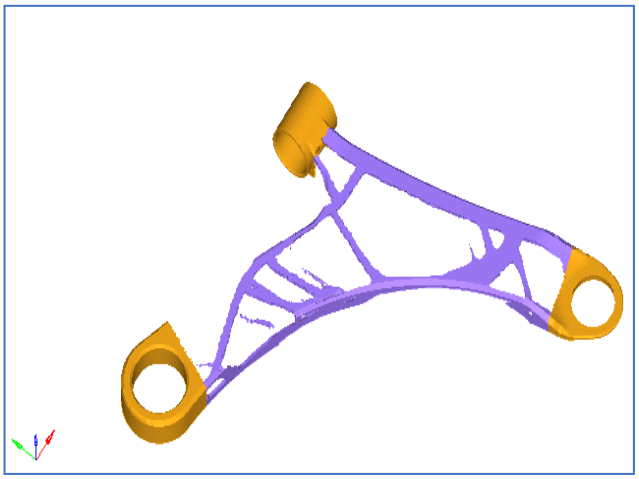

Figure: 4.4 Element Density Plot

Below figure 4.5 shows that low stress blue region can be removed from the design space while keep the red region in the design space as it is.

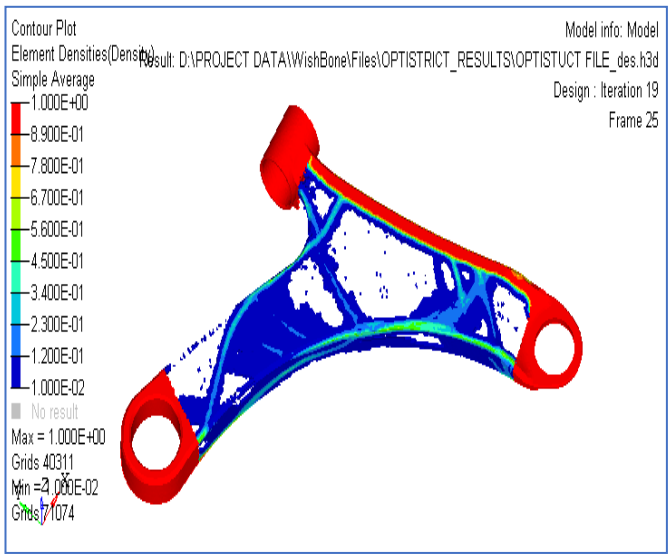

Figure: 4.5 Element Density Contour Plot

The optimized design is generated by extracting the raw material from the baseline design, based on the element density plot obtained through analysis. The optimized design, created using CATIA software, is depicted in Figure 4.6 and 4.7. These figures showcase the final design resulting from the optimization process.

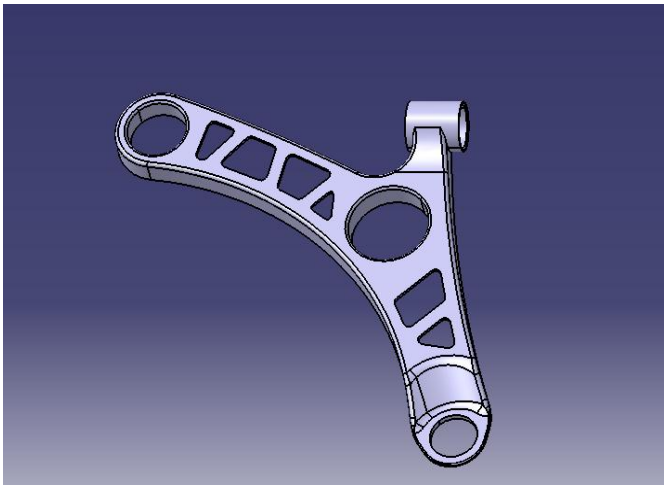

Figure: 4.6 Top view of Optimized Model of LCA

The mass of the optimized design is determined to be 1.03 Kg, as illustrated in Figure 4.21. This indicates a decrease in mass from the initial value of 1.2 Kg to 1.03 Kg. Consequently, the total percentage reduction in mass is calculated to be 15%.

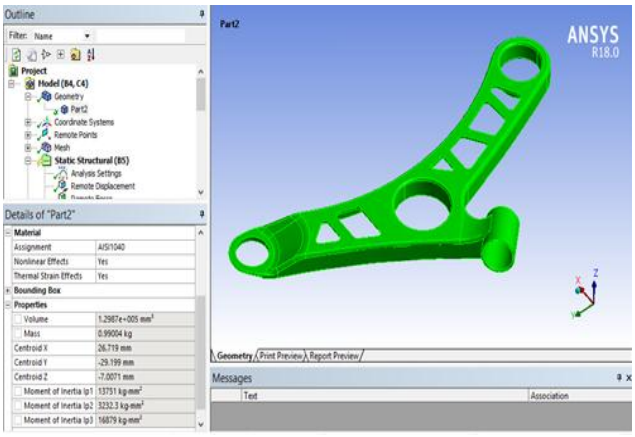

Figure: 4.7 Geometric properties of optimized lower control arm

4.3Meshing of Optimized Model:

The optimized model of the control arm is meshed using solid elements in ANSYS software. To generate the mesh, solid tetrahedral elements are employed for the control arm. Figure 4.8 illustrates the meshing of the optimized model of the lower control arm.

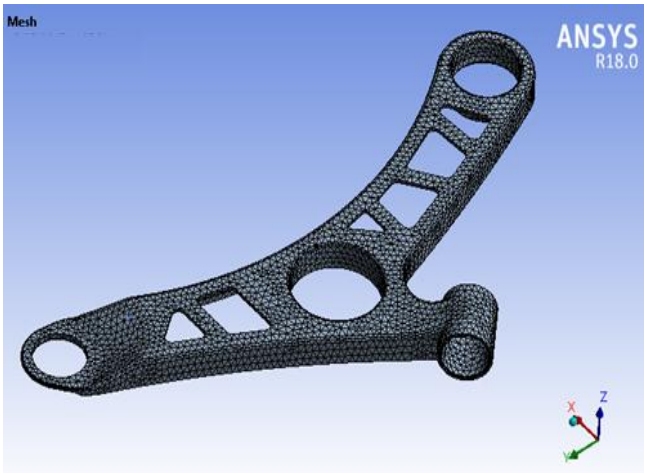

Figure: 4.8 Meshing of Optimized Model of LCA

4.4 Boundary Conditions of Optimized Model:

The boundary conditions applied to the optimized model are identical to those applied to the baseline model. A force of 750 N is applied at the remote location C of the lower control arm. Figure 4.9 depicts the boundary conditions of the optimized model, showcasing the applied forces and constraints.

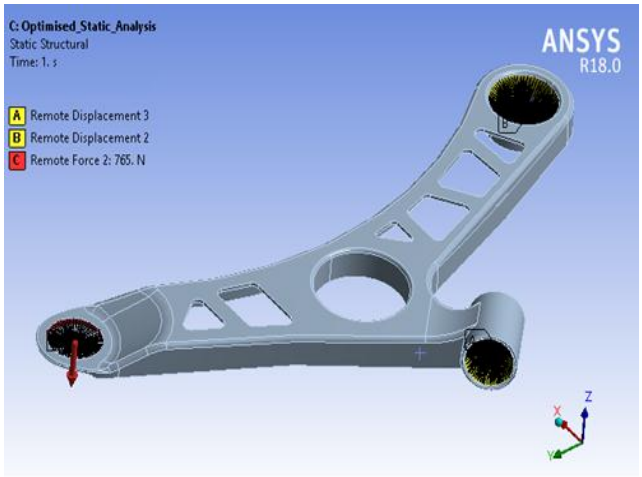

Figure: 4.9 Boundary Conditions of Optimized Model

4.5 Deformation Analysis of Optimized Model:

Following figure 4.10 shows the deformation plot of optimized design. The maximum deformation for the optimized design is observed up to 6.23 mm.

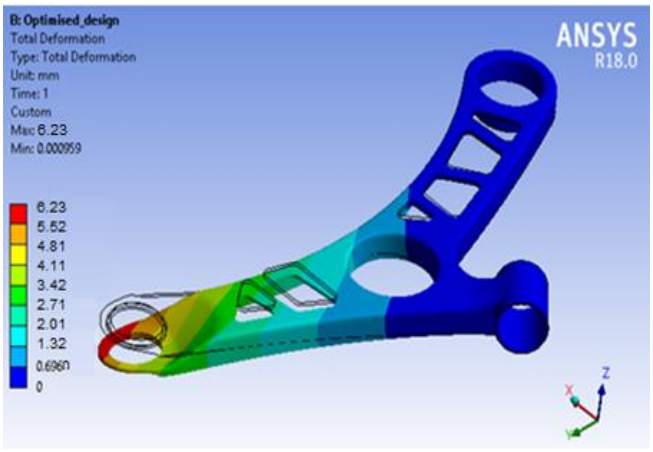

Figure: 4.10 Deformation Plot of Optimized design

.4.6Equivalent Stress Analysis of Optimized Model:

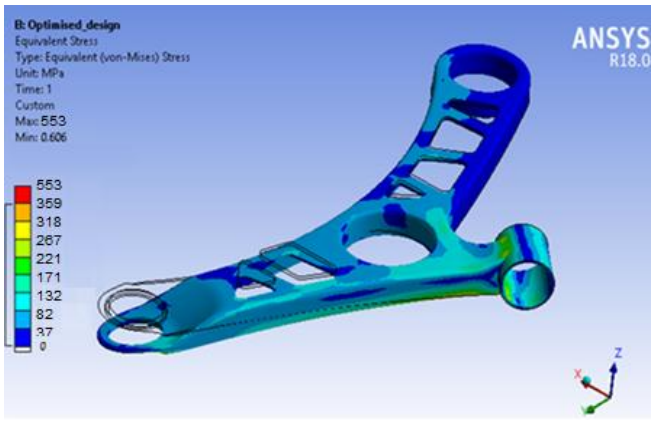

Figure: 4.11 Equivalent stress plot of Optimized design

Above figure 4.11 shows the Equivalent stress plot of Optimized design. The von-Mises stress is observed upto 371 Mpa for optimized model.

4.7 Factor of Safety of Optimized Model:

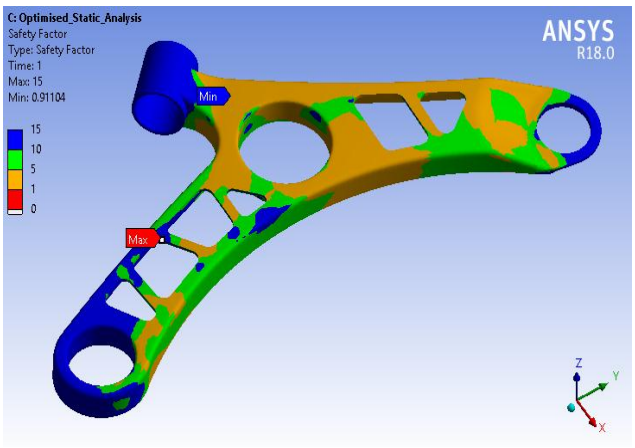

Figure: 4.12 Safety factor for optimized design

The plot of the factor of safety for the optimized model, as shown in Figure 4.12, indicates that all sections of the lower control arm have a factor of safety greater than 1. Additionally, certain portions of the arm exhibit a factor of safety ranging from 5 to 10. This suggests that the optimized model is deemed safe under the specified working conditions.

Considering the material's yield strength of 415 MPa, the analysis results demonstrate that the von-Mises stress is 371 MPa, which is lower than the yield strength. Consequently, the factor of safety for the optimized lower control arm is calculated as 1.1.

Table 4.1 provides a comprehensive overview of the FEA result analysis for the optimized model, offering additional details and insights.

Table 4.1 FEA Result Analysis of Optimized model

Method	Description	Optimized Design
FEA Method	Deflection, mm	6.23
	Von-Mises stress, MPa	371
	Factor of safety	1.1
	Mass, Kg	1.03

5. EXPERIMENTAL TESTING

5.1 Compression Test

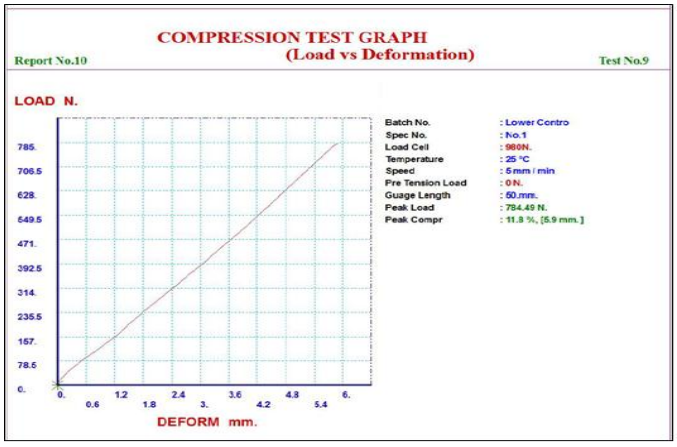

Figure: 5.1 Test Report Graph plot of Load vs. Deformation for Optimized Model

The analysis reveals that the maximum deformation for the optimized model is measured at 5.68mm. As the applied load increases, the deformation of the optimized model varies accordingly until it reaches a certain value. Similarly, the baseline model exhibits a deformation of up to 5.64mm. Both models demonstrate deformation behavior under the applied load, with the optimized model showing a slightly higher maximum deformation compared to the baseline model.

5.2 Strain Gauge Test

The reading obtained from strain gauge test is as shown in table 5.1 below.

Table 5.1 Strain Gauge Reading with Stress and Factor of safety calculation

Description	Baseline Design	Optimized Design
Strain (micron)	1550	1685
Stress (MPa)	326	351
Factor of Safety	1.27	1.17

6. DISCUSSION OF RESULTS AND VALIDATION

6.1 Results and Discussion

Table 6.1 Result Analysis

Sr. No.	Method	Description	Baseline Design	Optimized Design
1	Experimental Method	Deflection, mm	5.64	5.68
2		Von-Mises stress, MPa	326	351
4	FEA Method	Deflection, mm	6.02	6.23
5		Von-Mises stress, MPa	344	371
6		Mass, Kg	1.2	1.03

Following graph shows the results of both models by Finite element method.

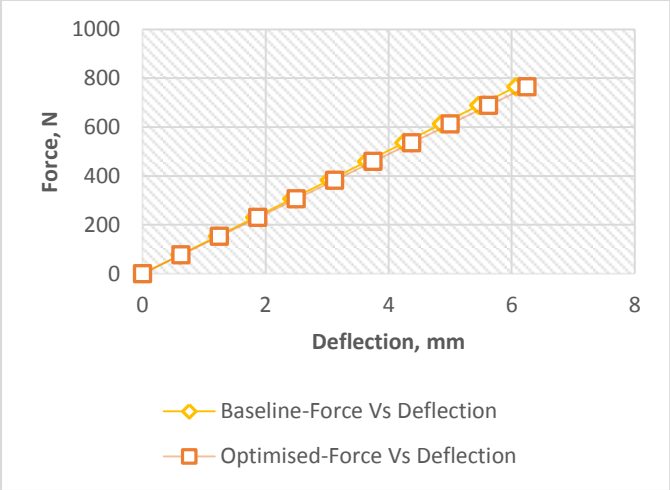

Figure: 6.1 Graph plot of Force vs. Deflection

Based on the graph presented in Figure 6.1, it can be observed that the deformation of the optimized model varies up to 6.25mm when subjected to a gradual application of load. This deformation is compared to the baseline model, showcasing the differences in deformation behavior between the two models under the same loading conditions.

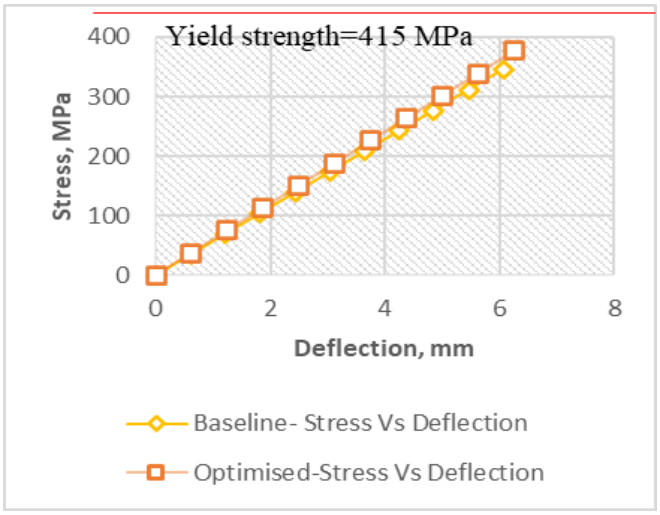

Figure: 6.2 Graph plot of Stress vs. Deflection

Upon analyzing the graph displayed in Figure 6.2, it is evident that the maximum stress induced in both the optimized and baseline models remains below the yield strength of the material. This observation confirms that the design is considered safe for the applied load conditions.

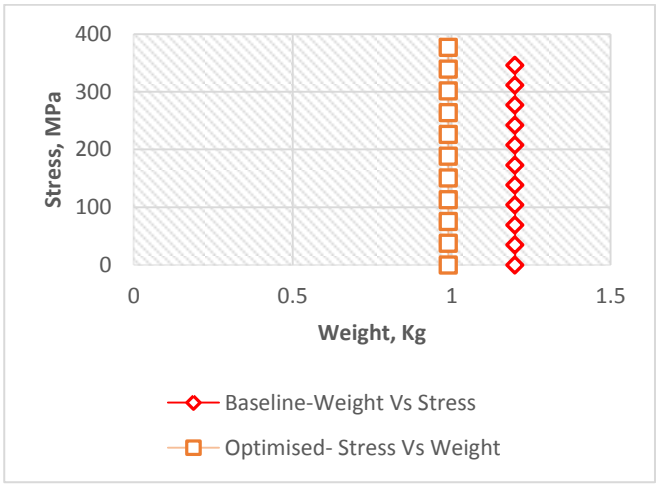

Figure: 6.3 Graph plot of Stress vs. Weight

Examining the graph depicted in Figure 6.3, it can be noted that there is an increase in stress within the optimized model as a result of the reduction in mass. However, it is important to emphasize that this increased stress remains below the yield limit of the material. Consequently, the design of the optimized model is considered safe despite the observed increase in stress.

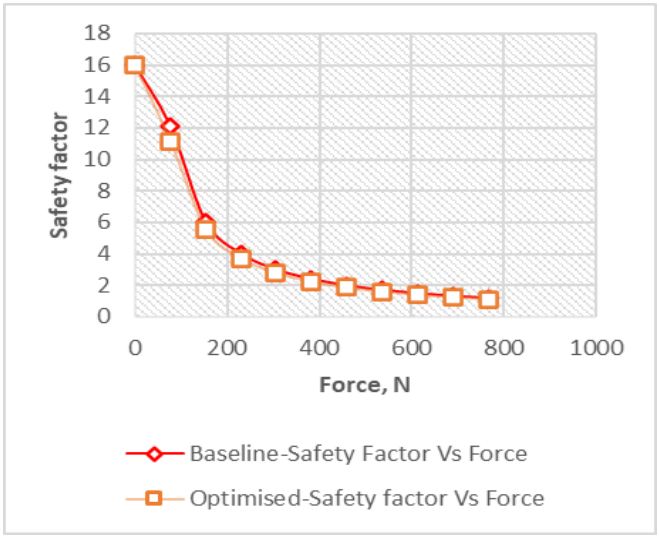

Figure: 6.4 Graph plot of Safety factor vs. Force

By examining the graph illustrated in Figure 6.4, it is apparent that a minor variation in the factor of safety, approximately 8%, can result in a significant reduction of 15% in the mass of a single lower control arm. This observation highlights the trade-off between the factor of safety and the weight reduction potential in the optimization process.

6.2 Validation

In this project validation is done by comparing ANSYS software results with experimental results of optimized model.

Table 6.2 Calculation of Percentage Error

Model	Description	Experimental Method	FEA Method	Percentage Error
Optimized Design	Deflection	5.68 mm	6.23 mm	8.10%
	Stress	351 MPa	371 MPa	6.49%

The FEA results are compared to the experimental results, yielding a percentage error of 8.1% and 6.49% for the deflection and stress of the optimized model, respectively. This comparison demonstrates a close convergence between the FEA predictions and the actual experimental measurements, indicating a good agreement between the two sets of results.

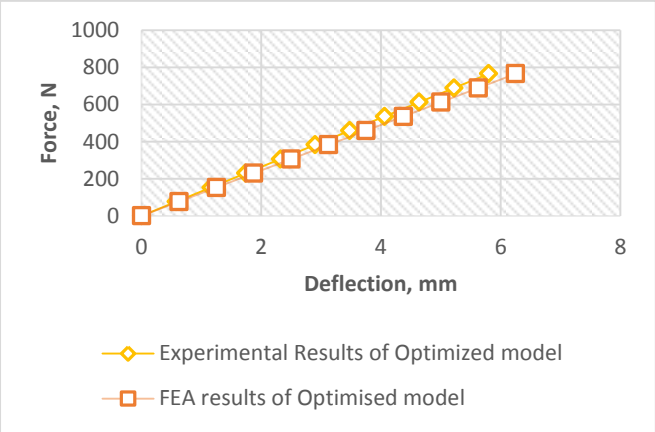

Figure: 6.5 Correlation Graph plot of Force vs. Deflection

Upon analyzing the graph displayed in Figure 6.5, it is evident that there is a correlation between the Force and Deflection values obtained from both the experimental and FEA methods. The comparison of these values reveals a percentage deviation of 8.1%. This indicates that the results obtained from the FEA method closely align with the experimental data, showcasing a strong correlation between the two approaches.

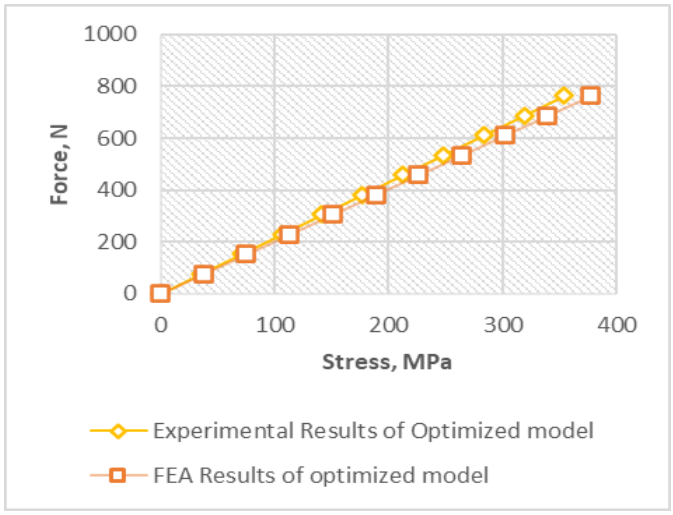

Figure: 6.6 Correlation Graph plot of Force vs. Stress

Upon examining the graph presented in Figure 6.6, it can be observed that there is a correlation between the Force and Stress values obtained from both the experimental and FEA methods. The comparison of these values reveals a percentage deviation of 6.49%. This indicates that the results obtained from the FEA method closely align with the experimental data, demonstrating a strong correlation between the two approaches.

7. CONCLUSION

The existing and optimized models of the lower control arm were subjected to static structural analysis in ANSYS Workbench, evaluating their stress and deformation under given boundary conditions. The deflection and stress levels observed in the optimized model were found to be within acceptable ranges, indicating that the modified design is safe for use. Furthermore, the weight of the final optimized model was measured to be 1.03 kg.

By achieving a 15% reduction in mass and material cost while maintaining a satisfactory factor of safety for the optimized design, the objectives of weight and cost reduction were successfully accomplished. The reduction in unsprung weight contributes to an increased ratio of sprung weight to unsprung weight, resulting in a smoother ride for the vehicle occupants. Moreover, a higher ratio of sprung weight to unsprung weight can positively impact vehicle control.

Overall, the weight reduction and cost optimization goals were met, leading to improved performance, ride quality, and control for the vehicle.

REFERENCES

[1] Prof. A. M. Patil et al"Experimental & Finite Element Analysis of Left Side Lower Wishbone Arm of

Independent Suspension System" IOSR Journal of Mechanical and Civil Engineering (IOSR-JMCE) e-ISSN: 2278-1684,p-ISSN: 2320-334X, Volume 7, Issue 2 (May. - Jun. 2013), PP 43-48.

[2] Rajashekhar Sardagi et al. "Design Analysis of Double Wishbone Suspension" IJRET: International Journal of Research in Engineering and Technology eISSN: 2319-1163 ,pISSN: 2321-7308 Volume: 03 Special Issue: 03,May-2014 NCRIET-2014.

[3] Vinayak Kulkarni et al. "Finite Element Analysis and Topology Optimization of Lower Arm of Double Wishbone Suspension using RADIOSS and Optistruct" International Journal of Science and Research (IJSR) ISSN (Online): 2319-7064 Volume 3 Issue 5, May 2014

[4] Sagar Darge et al. "Finite Element Analysis and Topography Optimization of Lower Arm of Double Wishbone Suspension Using Abacus and Optistruct" International Journal of Engineering Research and Applications .ISSN : 2248-9622, Vol. 4, Issue 7(Version 6), July 2014, pp.112-117.

[5] Jagwinder Singh et al. "Static Structural Analysis of suspension arm using Finite Element Method" IJRET: International Journal of Research in Engineering and Technology eISSN: 2319-1163,pISSN: 2321-7308 Volume: 04 Issue: 07 July-2015.

[6] Sarvadnya Ajinkya Thakare et al. "Design and Analysis of Modified Front Double Wishbone Suspension for a Three Wheel Hybrid Vehicle" Proceedings of the World Congress on Engineering 2015 Vol II WCE 2015, July 1 - 3, 2015, London, U.K.

[7] Balasaheb Gadade et al. "Design, analysis of A-type front lower suspension arm in Commercial vehicle" International Research Journal of Engineering and Technology (IRJET) e-ISSN: 2395-0056 Volume: 02 Issue: 07 , Oct-2015.

[8] Nikita Gawai et al. "Design, Modelling& Analysis of Double Wishbone Suspension System "International Journal on Mechanical Engineering and Robotics (IJMER) ISSN (Print) : 2321-5747, Volume-4, Issue-1,2016